# Femtosecond Ablation of Silicon in Acetone: Tunable Photoluminescence from Generated Nanoparticles and Fabrication of Surface Nanostructures

Syed Hamad,[†] G. Krishna Podagatlapalli,[‡] V. S. Vendamani,[†,§] S. V. S. Nageswara Rao,[†] A. P. Pathak,[†] Surya P. Tewari,[†,‖] and S. Venugopal Rao*[,‡]

[†]School of Physics and [‡]Advanced Center of Research in High Energy Materials ACRHEM, University of Hyderabad, Hyderabad 500046, India

[§]Department of Physics, Pondicherry University, Puducherry 605014, India

ABSTRACT: Silicon (Si) nanoparticles (NPs) and self-organized high spatial frequency laser (HSFL) induced periodic surface structures were fabricated by means of femtosecond ablation of bulk Si target in acetone. The ablation was performed with ~40 fs (fwhm) pulses and different input energies of ~500, ~200, ~150, ~100, ~50, and ~10 μJ. Fabricated NPs and nanostructures (NSs) were characterized by UV−visible absorption spectroscopy, photoluminescence (PL) spectroscopy, Raman spectroscopy, transmission electron microscopy, and field emission scanning electron microscopy. The average sizes of the NPs were estimated to be in the 4−135 nm range. From the PL studies of Si NPs of different sizes, we have observed a size-dependent shift toward blue spectral region. We could tune the observed PL peak in the spectral range of 440−515 nm. The crystalline and amorphous nature of the Si nanoparticles and nanostructures was investigated using selected area electron diffraction and Raman spectra. Complex refractive index, conduction band electron density of the Si NPs, estimated by measuring the effective spot size corresponding to each input energies, were observed to play a crucial role in determining the periodicity of HSFL induced periodic surface structures. Experimentally measured periodicity of gratings was in good agreement with the theory.
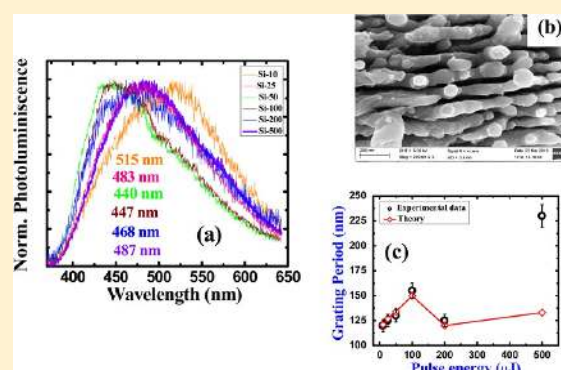
INTRODUCTION

Semiconductor nanoparticles (NPs) have been attractive candidates for their applications toward the fabrication of new materials such as optical gain media,[1,2] nanocrystalline based solar cells,[3] light emitting diodes,[4,5] bioimaging processes,[6,7] and photonics[8] due to their unique properties compared to the bulk. The optical, electronic, and structural properties of semiconductor NPs and nanostructures (NSs) are purely size dependent. When the dimensions of material are confined to nanoscale, energy spectrum turns discrete resulting in enlargement of the material's band gap. The properties of nanomaterials deviate significantly from those of bulk and isolated molecules. Silicon (Si) NPs are promising because of their outstanding properties resulting in applications in a variety of fields such as optoelectronics, photovoltaics,[9] and biomedical fields.[10,11] Si is an indirect band gap semiconductor material with an intrinsic band gap, which ranges in the infrared region. Phonons play an important role in the process of optical transitions in bulk silicon. When bulk Si is reduced to nanoscale, the zero-phonon optical transitions are moderately permitted. These zero-phonon optical transitions increase the radiative recombination rate through a band-to-band recombination process.[12−14] In Si NPs enlargement of energy difference between the eigen states leads to increased band gap. Consequently quantum confinement effects[15,16] render efficient photoluminescence (PL) in the visible region.[17,18] Especially, Si NPs being microelectronic compatible photonic materials have attracted more attention due to their size dependent PL with the prosperity of silicon surface chemistry.[19] Additionally, luminescent Si NPs are capable materials of demonstrating large third order nonlinear response[20,21] and possess potential for specific applications such as second harmonic generation.[22]

Silicon NPs have been fabricated through a variety of techniques such as sol−gel synthesis,[23] vapor deposition,[24,25] rf sputtering,[26] heavy ion irradiation,[27] microemulsion route,[28] and several other chemical and physical methods. Among all these techniques for manipulation of bulk materials to nanoscale, laser ablation in liquid media (LAL)[29−38] is one of the fast, simple, and versatile methods. Furthermore, LAL guarantees extremely stable NPs without using any capping agents with a highest degree of occupation. Particularly, ultrashort pulsed laser ablation (ULA)[39−43] is a unique material

processing technique that provides distinct advantages in applications over the nanosecond and continuous wave (cw) laser ablation. In addition, ultrashort laser pulses allow less thermal damage and a nearly melt free ablation, if carried out close to ablation threshold. Owing to the large peak intensities associated with picosecond (ps) and femtosecond (fs) laser pulses, absorption involves multiphoton processes. Furthermore, within ps and fs time scales the energy cannot be transferred from electron to the lattice instantly. Thermal descriptions maintain individuality between electron and lattice temperature. Therefore, two-temperature model becomes necessary in order to describe thermal phenomena.[44] In the process of SiNPs fabrication, when an ultrafast pulse is incident on silicon target, valence band electrons can respond first to absorb visible/IR wavelengths and transitions occur from valence band to conduction band. In the case of fs pulses in the near IR region, linear and nonlinear absorption (multiphoton absorption) are the dominant mechanisms. Absorption of laser energy by the valence electrons creates quasi-free carriers.[45] The excited electrons transfer their energy to lattice through electron−lattice coupling, and the corresponding characteristic time is ∼1 ps. Collisions between the electrons and lattice leads to higher temperatures in the vicinity of laser focused regions, and consequently, material transits to a super critical fluid state, and vaporization occurs via the interaction of surrounding liquid media creating a multifaceted structure of nanomaterials.

Thus far people have reported the influence of pulse duration and pulse energies in size distribution of the fabricated Si NPs.[40,46] Among recent significant reports, Intartaglia et al.[46,47] had fabricated Si NPs in liquid media with ∼100 fs laser pulses at different pulse energies. The writing conditions in their experiments were different (laser beam was focused at a single point on the target) from our experiments. In our experiment, the focused laser pulses (∼40 fs, fwhm) were scanned on the surface of the Si substrate to draw periodic lines with a given separation rather than mere focusing. Furthermore, the scan separation between the structured lines was chosen in such a way as to ablate the preablated line on the material surface, two or multiple times, and is labeled as double/multiple line ablation (separation of 30 μm). Recently, our group has reported the fabrication of Ag NPs and NSs by ultrafast double line ablation.[48] In addition to NPs, laser induced periodic surface structures (LIPSS) in semiconductors have also been investigated using ps and fs lasers.[49−52] The phenomenon responsible for the formation LIPSS was extended to the fs regime about 10 years ago.[53] In this regime, LIPSS (spikes or ripples) can be produced when the laser fluence is approximately equal to the threshold fluence of the material. Recently, our group has reported the fabrication of aluminum NSs achieved through fs laser ablation of Al in water demonstrating the formation of subwavelength sized nano-ripples.[54] In the present article we report our results from the fs ablation studies of Si in liquid acetone. We have specifically investigated (a) pulse energy dependence of the average size of generated Si NPs, (b) PL studies of the created NPs, (c) formation of subwavelength LIPSS on the surface of Si, and (d) model our experimentally observed data for estimating the periodicity of LIPSS.

■ EXPERIMENTAL DETAILS

Si NPs and NSs were synthesized by ablating bulk silicon in acetone using 1 kHz chirped pulse amplified Ti:sapphire laser system (LEGEND, Coherent) delivering nearly bandwidth limited laser pulses of ∼40 fs pulse width at 800 nm. The amplifier was seeded with ∼15 fs pulses (bandwidth of 55−60 nm, fwhm) from an oscillator (MICRA, Coherent, 1 W, 80 MHz, 800 nm). The average power from the amplifier was ∼2.5 W. The initial laser beam of diameter 8 mm was focused on the surface of Si substrate with the help of a 25 cm focal length of the lens. The Boron doped-type Si (100) target with very low resistivity (<0.005 Ω-cm) was cleaned in an ultrasonic cleaner with acetone. The Si target was submerged under the acetone in a Pyrex cell, and the effective thickness of liquid layer above the Si target was ∼7 mm. Complete details of the experimental detail are reported in our earlier works.[55−57]

The theoretical beam waist ($2\omega_0$) estimated at the focal point in air was ∼40 μm. Typical range of pulse energies used was 10−500 μJ, and the input energy was controlled by a combination of Brewster angle polarizer and half wave plate. The target was placed normal to the laser beam on a three-dimensional motorized stage [Nanodirect] with a resolution of 25 nm. The X−Y stages were moved in such a way to draw periodic lines on the substrate with a separation of ∼30 μm using scanning speeds of 0.3 and 0.5 mm/sec in X and Y directions, respectively. Typical duration of each scan was ∼40 min. The refractive index and thickness of liquid (acetone) layer play a crucial role in affecting the laser fluence at the focus on the surface of the target. Consequently, the position of the focal plane shifted toward the target, which modified the beam waist on the target surface. Modification of beam waist results in deposition of less amount of fluence on the target. In the present case, focus was adjusted to be exactly on the surface of the target through compensating the shift caused by the presence of liquid layer following the procedure reported by Menendez-Manjon et al.[58] After completion of the scan, prepared colloids were collected in air tightened glass bottles. The substrates on which ablation was carried out were cleaned and preserved. To avoid the ambiguity, in addressing prepared colloidal Si NPs in acetone were designated as Si-500, Si-200, Si-100, Si-50, Si-25, and Si-10, and the corresponding substrates as SiS-500, SiS-200, SiS-100, SiS-50, SiS-25, and SiS-10 for pulse energies 500, 200, 100, 50, 25, and 10 μJ, respectively.

The surface morphology, structural properties, and elemental composition of the Si NPs were characterized by transmission electron microscopy (TEM), selective area electron diffraction (SAED), Raman spectroscopy, and energy dispersive X-ray analysis (EDAX), respectively. TEM, SAED, and EDAX were performed with FEI Tecnai G2 S-Twin200 kV instrument via placing a drop of Si NP colloids on carbon coated copper grids and incubated for 24 h to dry the sample at room temperature. The absorption shoulder peak position of Si colloidal solution was recorded by UV−visible absorption spectra with a Jasco V-670 instrument. A WITec Alpha 300 spectrometer was used to record the Raman spectra at an excitation wavelength of 532 nm (cw) and photoluminescence spectra with an excitation wavelength of 355 nm. A drop of Si NPs solution was placed on glass coverslip and allowed to dry for photoluminescence measurement. The sample on the coverslip can be easily identified through the in-built optical microscope (with an objective lens of 40×) and the spectrum was collected by the in-built detector in the WITec instrument simultaneously. To avoid the heating effect through the accumulation, low power (5 mW) was used for both studies. Similarly, surface morphologies of the laser exposed portions of the Si substrates were carried out through a scanning electron microscopy
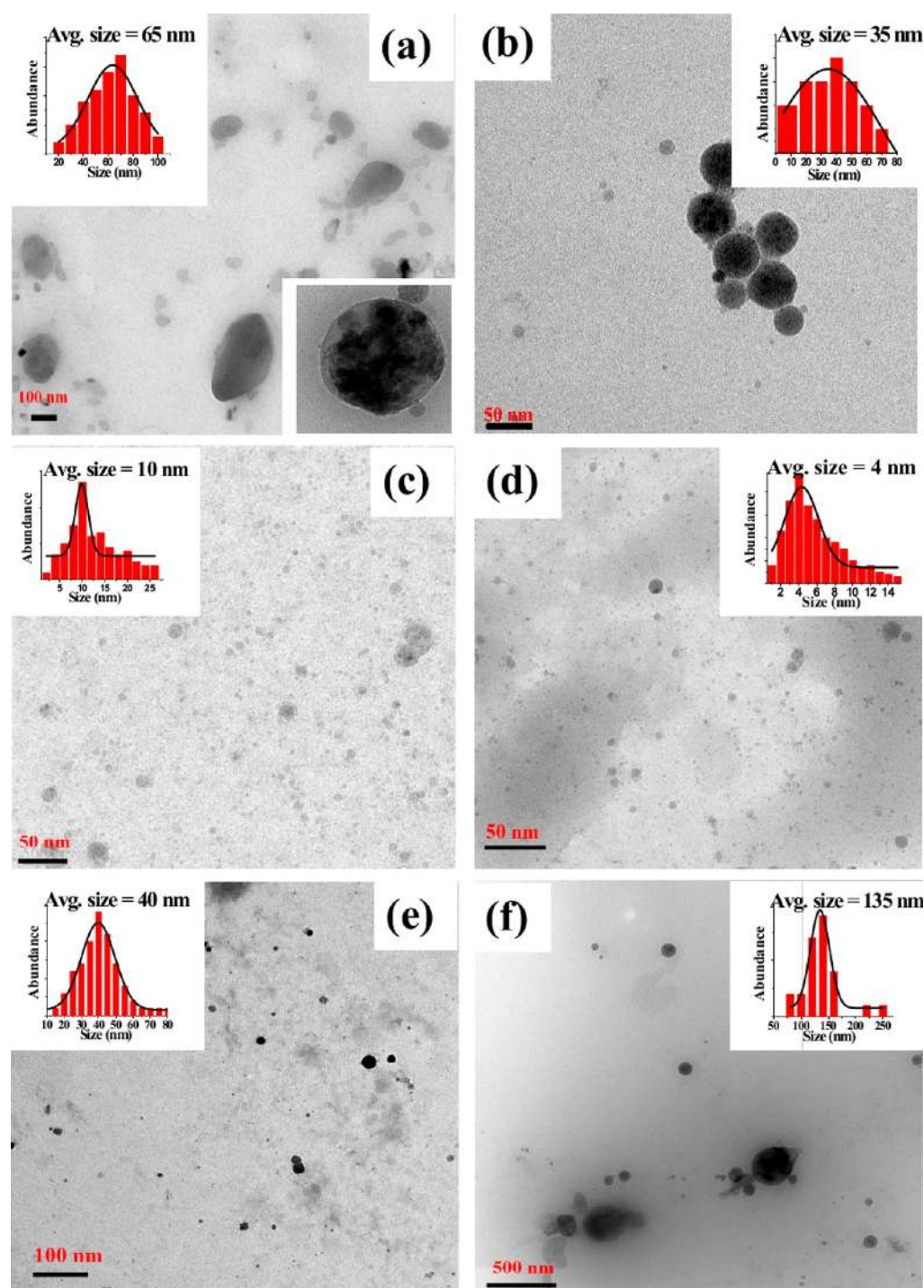
Figure 1. TEM images illustrate the Si NPs synthesized by fs laser ablation of bulk Si in acetone: (a) Si-500 (inset bottom shows core−shell type Si NP), (b) Si-200, (c) Si-100, (d) Si-50, (e) Si-25, and (f) Si-10. Insets show their particle distribution plots.

(SEM) [Ultra 55 from Carl ZEISS with 5 kV accelerating voltage] instrument.

■ RESULTS AND DISCUSSION

Characterization of Si NPs. Morphology and size distribution of the fabricated Si NPs were carried out by TEM measurements. From the TEM images presented in Figure 1, the shape of the particles seems mostly spherical in nature and different size distributions are observed for different pulse energies. These images confirmed the formation of nonagglomerated spherical nanoparticles in each case. Figure 1 represents the TEM images of colloidal Si NPs synthesized in acetone as a function of pulse energy. The insets of this Figure illustrate the histograms of size distribution with an average size ranging 20−100 nm in Si-500 [Figure 1a], 5−70 nm in Si-200 [Figure 1b], 2−25 nm in Si-100 [Figure 1c], 2−15 nm in Si-50 [Figure 1d], 15−80 nm in Si-25 [Figure 1e], and 80−250 nm in Si-10 [Figure 1f]. Gaussian fits of the histogram provided the average particle size of ∼65 nm for Si-500, ∼35 nm for Si-200, ∼10 nm for Si-100, ∼4 nm for Si-50, ∼40 nm for Si-25, and∼135 nm for Si-10. Average size was observed to decrease

as the pulse energy decreased from ~500 to ~50 μJ [Figure 1d]. However, the average size increased when the pulse energy was further decreased to ~10 μJ [Figure 1f]. Size distributions and yield of NPs depend solely on cavitation bubble dynamics arising from the target surface. Even the origin and complete dynamics of cavitation bubble followed by NPs fabrication are not clearly understood, especially in the ps/fs ablation case. From our knowledge and data from previous reports we understand that low input energies generate a sustainable cavitation bubble of smaller size, whereas at high input energies the cavitation bubble cannot sustain for long times. Consequently, in the latter case pressure developed across the bubble is less since it collapses instantaneously, which might produce agglomerates of large dimensions. However, in the former case, sustainability of the bubble develops higher pressures and, as a result, the collapse results in the formation of lower sized NPs.[59]

Figure 2 depicts the HRTEM image of a single Si nanoparticle (Si-50) exhibiting parallel Si lattice planes with
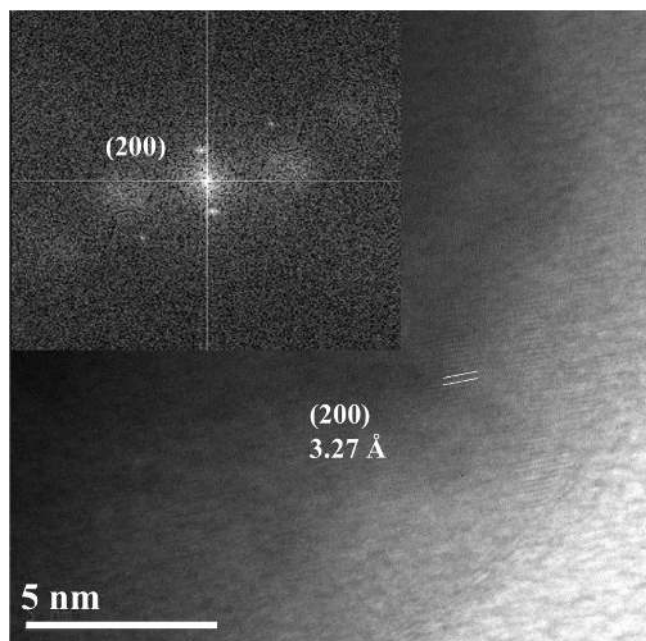

Figure 2. HRTEM image of Si NP depicting the clear view of lattice planes observed at a characteristic separation 3.27 Å, which corresponds to the plane of Si lattice set (200), and the inset shows its numerical electronic diffraction.

an interplanar separation of 3.27 Å (indicated with a white mark) corresponding to (200) lattice planes of Si. Figure 3 illustrates the SAED pattern of colloidal Si NPs in (a) Si-500, (b) Si-200, (c) Si-100, (d) Si-50, (e) Si-25, and (f) Si-10. The SAED pattern was observed to show concentric rings corresponding to individual lattice planes. The first three planes were considered for discussion in each pattern. The diffraction pattern for Si-500, Si-200, Si-100, and Si-50 confirmed that most of the Si NPs were observed to possess poly crystalline nature and that the pattern for Si-25 and Si-10 revealed single crystalline nature of the Si NPs. Figure 3 illustrates SAED patterns, and measured interplanar spacings agree very well with respective Si crystal planes in the literature. In addition to this, we observed one more lattice plane with a spacing of 1.59 Å, which agrees with the $SiO_2(220)$ plane in Si-500 [Figure 3a], and 2.97 Å, which agrees with SiO_2 (110)

plane in Si-200 [Figure 3b]. Insets of Figure 3 demonstrate the EDAX spectra of colloidal Si NPs. The peaks associated with Si and oxygen were observed in all cases (pulse energies) except for Si-50 and Si-100 samples. This confirmed that Si NPs were successfully generated without any significant impurities.

Raman spectroscopy provides crystalline/amorphous information of Si NPs. Figure 4 depicts the Raman spectra of Si-10, Si-25, Si-50, Si-100, Si-200, and Si-500. Si-50, Si-100, and Si-200 s were observed to have both amorphous and crystalline nature through the exhibition of 484 cm^{-1} as well as 512.3 cm^{-1} Raman signatures in the spectra. Similarly, Si-10, Si-25, and Si-500 exhibited crystalline phase through elevation of the 516.9 cm^{-1} mode, typical of nanocrystalline Si. To avoid confusion in peak positions, each spectrum in Figure 4 was shifted vertically for better comparison. From these plots, the peak position, representing the crystallinity of Si NPs, was observed to shift toward lower wavenumber region along with the broadening of Si crystalline peak, as the particle size decreased.[60−62] As evident from the Raman spectra (Figure 4), signatures in the 470−492 cm^{-1} region, a prominent amorphous peak was observed at 484 cm^{-1} for Si-200, Si-100, and Si-50. A sign of such phase was not observed for other Si NPs (Si-500, Si-25, and Si-10) and pure Si wafer. The peak position at 520.8 cm^{-1} (crystalline) of pure silicon wafer was taken as a reference for quantifying the peak shift observed in this study. The shift to lower wavenumber region and strong asymmetry observed when the input energy decreased from 500 μJ (Si-500) to 50 μJ (Si-50) could be from phonon confinement[63] in the nanocrystals and amorphous contribution (484 cm^{-1}). With further decrease in pulse energy from 50 μJ (Si-50) to 10 μJ (Si-10), lesser asymmetry was observed, which could be due to low amorphous phase of Si NPs,[64] and this, possibly, could be the reason for increased sizes of Si NPs. In the course of ablation beneath the liquid molten layer, Si is subjected to an abrupt cooling (of ~10^{13}−10^{15} K/s), which provokes resolidification of the molten droplet. This kind of rapid cooling, and hence the solidification, leads to the observed amorphization. In general, two kinds of amorphization of Si NPS were observed by earlier groups: (a) core−shell type in which amorphous silicon (SiO_x) acts as shell on the core crystalline Si and (b) complete amorphization of Si, which is particular for the particle dimensions less than 10 nm.[65,66]

The fabricated colloidal Si NPs possessed strong absorption band in the UV spectral region. Figure 5 illustrates the UV−visible absorption spectra of Si NPs in acetone. A methodical blue shift was observed in peak position of absorption spectra with respect to a decrease in average size of NPs, which demonstrates that the band gap of NPs increased. Si NPs in Si-500 showed a strong absorption peak positioned at ~338 nm and a broad peak near 400 nm. When the pulse energy was decreased the peak position shifted toward shorter wavelength side (blue-shifted) along with an increase in the peak intensity. Beyond a certain increase in energy, the position of absorption peak was red-shifted (for larger particles). The shifted absorption peak positions were 316 nm (Si-200), 308 nm (Si-100), 304 nm (Si-50), and 336 nm (Si-25). In the case of Si-10, a broad continuous band between 340−800 nm (mean size of NPs was ~135 nm) with a broadened peak near ~420 nm was observed. The broad continuous band is attributed to the broad distribution in size of fabricated NPs. The occurrence of UV band absorption for Si NPs with smaller size was reported earlier.[67] Intartaglia et al.[68] have studied the
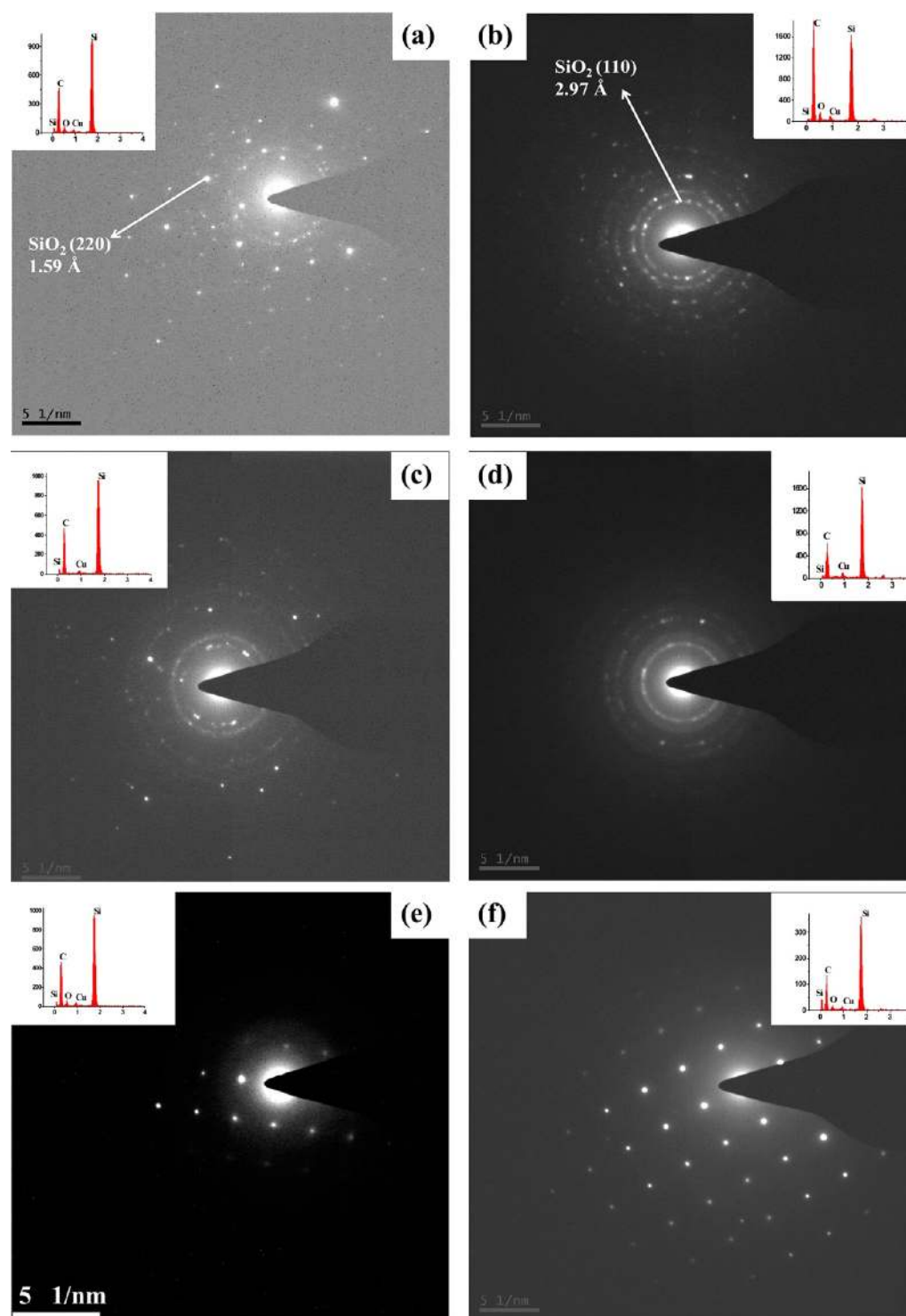
Figure 3. SAED pattern descriptions illustrate the Si NPs synthesized by fs laser ablation of bulk Si in acetone: (a) Si-500, (b) Si-200, (c) Si-100, (d) Si-50, (e) Si-25, and (f) Si-10. Insets show their respective EDAX images.

absorption band near 300 nm and attributed it to the carbon byproducts.

PL measurements were carried out for the fabricated colloidal Si NPs by depositing them on a glass slide (coverslip), and the results are presented in Figure 6. For the purpose of comparison, PL intensity was normalized at the peak position. Shifting of the PL peak position with respect to the average size of the Si NPs was observed, and the data is plotted in Figure 7. PL peak position was observed to have blue-shift for decreasing

energies in the 500−50 μJ range. However, it was red-shifted for decreasing energies in the 50−10 μJ range. It was observed that the position of the PL peak purely depended on the size of NPs. First, the position of the PL peak was tuned from 483 to 440 nm and later from 440 to 515 nm. The tuning range of PL spectrum from 483 to 440 nm is attributed to decrease in the size of NPs, which could be from quantum confinement effects.[69] PL observed in the spectral range of 440−515 nm can possibly be attributed to increase in the size of particles, which
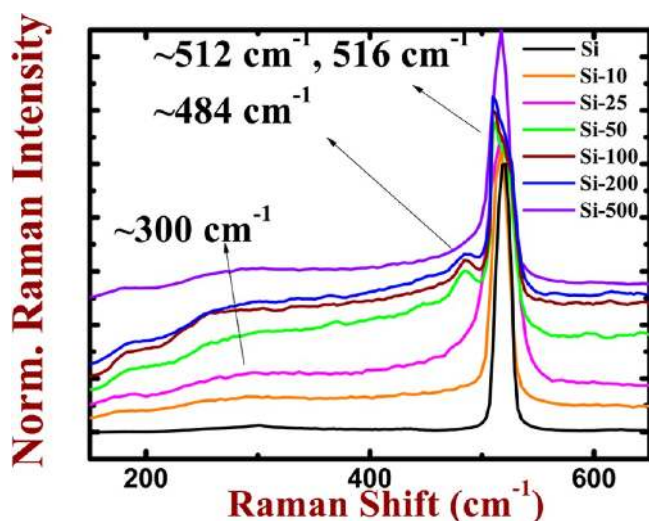
Figure 4. Raman spectra of Si NPs (prepared in acetone) in (i) Si-500, Si-25, and Si-10 with crystalline peak around 516 cm^{-1}, (ii) Si-200, Si-100, and Si-50 with crystalline peak around 512 cm^{-1} and amorphous peak around 484 cm^{-1}, and (iii) bulk Si with crystalline peak at 520 cm^{-1}.

Figure 6. Photoluminescence spectra of Si NPs (prepared in acetone) in (i) Si-500 with emission peak at 487 nm, (ii) Si-200 with emission peak at 468 nm, (iii) Si-100 with emission peak at 447 nm, (iv) Si-50 with emission peak at 440 nm, (v) Si-25 with emission peak at 483 nm, and (vi) Si-10 with emission peak at 515 nm.
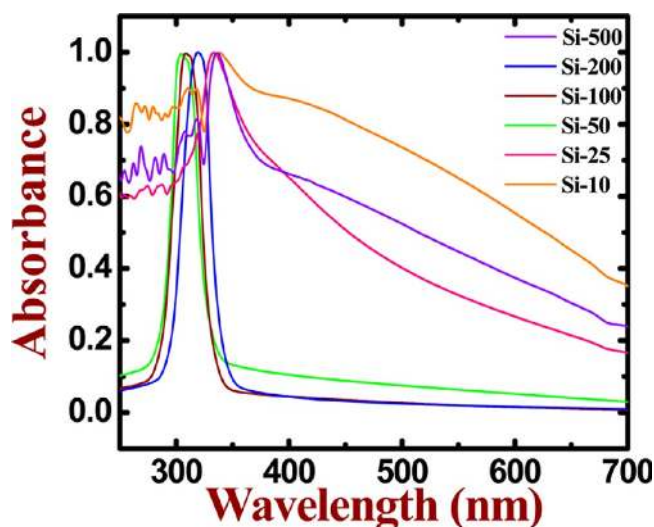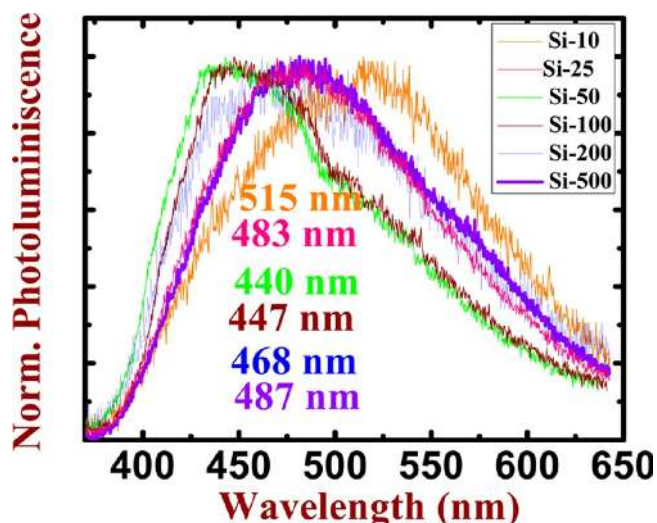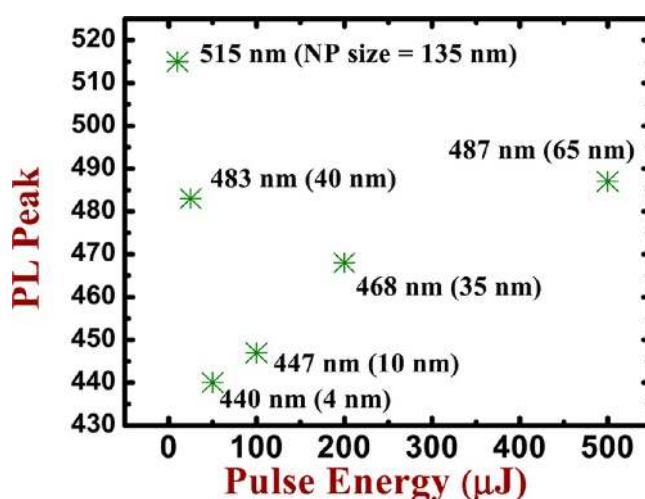

Figure 5. UV−vis absorption spectra of Si NPs (prepared in acetone) in (i) Si-500 with shoulder peak at 338 nm (broad peak around 400 nm), (ii) Si-200 with shoulder peak at 316 nm, (iii) Si-100 with shoulder peak at 308 nm, (iv) Si-50 with shoulder peak at 304 nm, (v) Si-25 with shoulder peak at 336 nm, and (vi) Si-10 shoulder peak 340 and strong broad peak at ∼420 nm.

Figure 7. Plot depicts the tuning of emission peak of Si NPs prepared in acetone with respect to the pulse energy.

is a result of diminishing quantum confinement effect. Many earlier reports discuss the PL of Si NPs in the visible spectral region of 400−590 nm.[68,70−73]

Characterization of Silicon Substrates. Inherent nature of the silicon nanostructures was evaluated by recording the Raman spectra. The crystalline (amorphous) nature of the NSs induced by fs pulses on Si substrate was characterized by a Raman spectrometer (WI-Tec instrument) using 532 nm excitation. Inspection of the Raman plots of the NSs on SiS-500, SiS-200, SiS-100, SiS-50, SiS-25, and SiS-10, and bulk Si illustrate the similar pattern to that of NPs and comparison of the plots in regions determined as crystalline and amorphous phases, as shown in Figure 8. Raman spectra showed a shift toward lower wavenumber and broadening of 520 cm^{-1} peak

for all NSs suggesting the presence of nanocrystalline Si. Furthermore, a prominent peak was also observed near 470 cm^{-1}, which could be from amorphous nature of NSs formed on Si substrate for all the cases.

The surface morphology of the ablated area of the Si substrates was characterized by FESEM imaging. Figure 9 depicts the FESEM images of formed laser induced periodic surface structures (LIPSS) with high spatial frequency (HSF) via femtosecond laser double/multiple line ablation on Si substrates (a) SiS-500, (b) SiS-200, (c) SiS-100, (d) SiS-50, (e) SiS-25, and (f) SiS-10. In some of the earlier studies,[74−84] few probable mechanisms were proposed to explain the production of low spatial frequency (LSF) LIPSS with a period of nearly half of the laser wavelength and high spatial frequency (HSF) LIPSS with period much less than the incident wavelength of laser achieved via fs laser ablation. Gemini et al.[79] reported self-organized structures with spatial periodicity of ∼600 nm on Si using laser fluences just above the ablation threshold. They, however, irradiated the target with a large number of pulses.
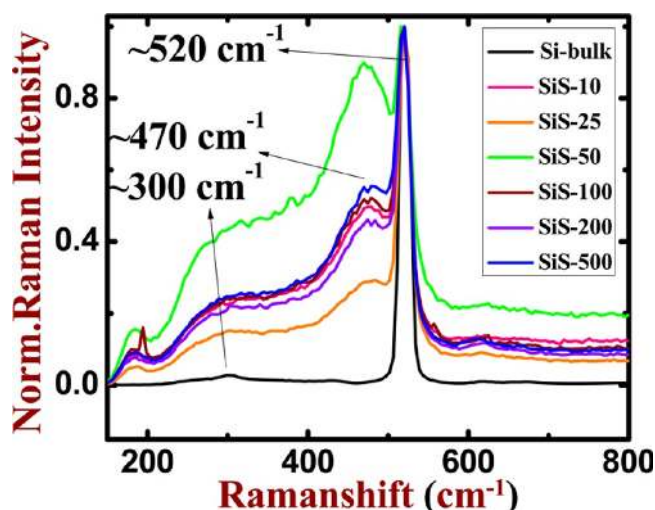
Figure 8. Raman spectra of HSFL (nanostructure) on the Si substrates depict asymmetric crystalline peak around 520 cm^{-1}, amorphous peak around 470 cm^{-1}, and bulk Si with crystalline peak at 520 cm^{-1}.

The dependence of spatial periodicity on laser fluence was accounted by the parametric decay of laser light into surface plasma waves. Miyazaki et al.[80] investigated the fundamental mechanisms of fs laser induced periodic surface nanostructure formation in diamond-like carbon and GaN and demonstrated that the nanostructure formation can indeed be controlled. Derrien et al.[81] investigated the mechanisms of ripple formation on Si using fs pulses and demonstrated the transient evolution of density of the excited free-carriers. Liu et al.[82] presented an interesting anisotropy phenomenon observed in fs laser processing of crystalline Si. Their results indicated that the surface patterning was dependent on the input laser polarization. In most of the earlier studies the mechanisms were discussed for ablation performed in air/vacuum, whereas in our case we performed ablation in liquid. In the present case, HSFLIPSS (HSFL) with an increased periodicity was observed as the pulse energy decreased from 500−10 μJ and was confirmed from the FESEM images. A closer look at the images ascertained that Si NP grains were observed on top of the HSFL. The mechanism of the formation of HSFL could be explained from the changes in physical properties of material, i.e., the complex refractive index. When silicon absorbs fs pulses it results in the formation of quasi-free electrons in the conduction band of solid Si in a time scale <1 ps (electron−phonon recreation time). Absorption of incident light by the valence band electrons and formation of quasi-free electronic states modify the complex refractive index ($\mathbf{n}*$) of the excited state and conduction band electron density (N_e). According to the Drude model,[85,86] complex refractive index and conduction band electron density are related by the following equation

$$\mathbf{n}* = \sqrt{n^2 - \frac{N_e e^2 \tau_d^2}{\varepsilon_0 m_{eff} m_e \left(\frac{4\pi^2 c^2}{\lambda^2}\tau_d^2 + 1\right)}} \quad (1)$$

where e is charge of electron (= 1.6×10^{-19} c), m_e is the electron mass (= 9.11×10^{-31} kg), λ is the wavelength of the laser (= 800 nm), $\varepsilon_0 = 8.85 \times 10^{-12}$ Fm^{-1}, c is the velocity of light (= 3×10^8 m/sec), n is the refractive index, which depends on wavelength (λ) (= 3.675 at 800 nm), m_{eff} = effective mass of carriers occurred after the excitation (0.18),

and τ_d is Drude's damping time constant for excitation of silicon in fs regime (= 1 fs). These values have been taken from published literature.[84,86] N_e is the electron density in the conduction band.

The estimation of electron density (N_e) in the conduction band under fs laser excitation of silicon, which depends on the laser fluence (intensity) along with the changes of linear and nonlinear absorption phenomena occurring after fs excitation were explained earlier by Harzic et al.[86] using the following relationship:

$$N_e \approx F\frac{\lambda(1-R)}{hc}\left[\alpha_0 + \beta F\frac{(1-R)}{2\sqrt{2\pi t_p}}\right] \quad (2)$$

where R is the surface reflectivity of silicon parallel to the normal (= 0.329)[87] and α_0 and β are the linear and nonlinear absorption coefficients of silicon, respectively. Values of α_0 (1×10^3) and β (6.8×10^{-9} cm/W) in the fs regime were considered from earlier reports.[88] Effective pulse duration estimated was $t_p \approx 70$ fs at the site of sample (effect of dispersion in pulse length when pulse passes through the media), h is the Planck's constant, and F is the fluence of laser pulses used to ablate the solid.

The observation of HSFL structures are explained on the basis of complex refractive index (n_e*) and conduction band electron density (N_e). It was observed that N_e was directly related to the fluence of the laser on the target surface and $n*$ directly depends on the N_e. From the theoretical base both $n*$ and N_e were observed to have a direct dependence on the laser fluence. To investigate the effect of fluence on the formation of the HSFL on silicon surface, effective spot size on the silicon target for different input energies was estimated experimentally. Microscopic images of laser drawn single lines on silicon surface are shown in Figure 10. Barcikowski et al.[89] demonstrated that the width of line structure on the ablated surface was considered as the effective beam waist of the laser beam. Figure 10 confirmed the differences in effective spot size (width of the line) even when the experiment was carried out at similar conditions of liquid level above the target and position of focus except the input laser pulse energy. From the data presented in Figure 10, estimated spot sizes were ~60, ~80, ~100, ~120, ~270, and ~320 μm for the input energies of ~10, ~25, ~50, ~100, ~200, and ~500 μJ. Figure 11a depicts estimated spot sizes and corresponding fluences for each input laser energy. From the estimated spot size and number of pulses per spot and separation between the lines, we confirmed that double line ablation occurred on SiS-10 and SiS-25 since the separation (30 μm) between the lines was almost half compared to the spot size on the target. Consequently, half of the ablated line was again exposed to the laser beam ablating it for the second time.[48] An effective number of pulses calculated [from $\omega(z)/d$ where d is pulse spacing] was ~400 and ~540 per spot on SiS-10 and SiS-25, respectively. In the case of SiS-50, SiS-100, SiS-200, and SiS-500, the estimated spot size was much greater than the separation with corresponding fluences at the point of ablation on the target being ~0.35, ~0.5, ~0.63, ~0.88, ~0.34, and ~0.6 J/cm^2, respectively. Consequently, overwriting of the surface took place and the effective number of laser pulses per spot estimated was ~990, ~1600, ~4500, and ~5000, respectively.

On the basis of the variations in the scheme of ablation, effective fluence (spot size and number of pulses) on the Si surface, better yield of NPs [data presented in Figure 1] was
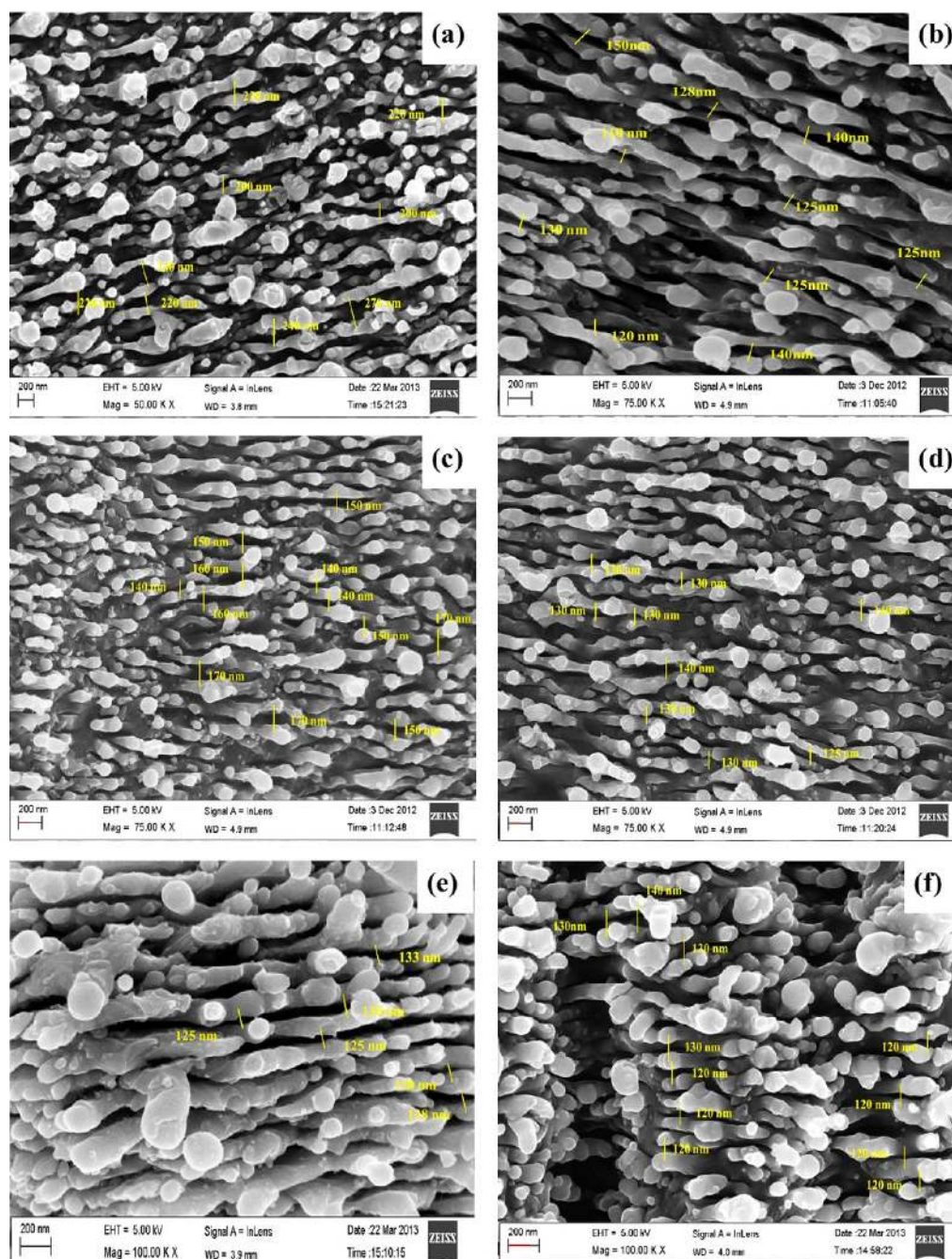
Figure 9. FESEM images of HSFL structures were fabricated on Si substrate by fs laser ablation of bulk Si in acetone: (a) SiS-500, (b) SiS-200, (c) SiS-100, (d) SiS-50, (e) SiS-25, and (f) SiS-10.

obtained in the case of Si-50 and Si-100. However, in the case of Si-10, Si-25, and Si-200, the estimated fluence was near to the ablation threshold of silicon, and therefore, we could see a mere ablation. In the case of Si-500 the dynamics of ablation were unexpected. As the estimated spot size (∼320 μm) at this fluence on the silicon surface was much greater than the given separation between the lines (30 μm), overwriting of the surface could have occurred many times up to the level of saturated ablation, which is designated as multiple ablation. Consequently, we could not obtain better yield of NPs, and correlation between the theoretical and experimental estimations of periodicity failed. Similarly, differences in effective number of laser pulses on the silicon surface led to the production of nanograting with an average periodicity on SiS-

10, SiS-25, SiS-50, SiS-100, SiS-200, and SiS-500 being ∼120, ∼125, ∼130, ∼155, ∼125, and ∼230 nm, respectively. These values are in good agreement with the theoretically calculated ($\Lambda = \lambda/2n^*$) period of the gratings of ∼121, ∼127, ∼134, ∼150, ∼120, and∼133 nm for the substrates SiS-10, SiS-25, SiS-50, SiS-100, SiS-200, and SiS-500, respectively. Theoretical estimation of the grating periodicity was carried out by estimating the electron densities of the conduction band (N_e) and complex refractive index (n^*), which are tabulated in Table 1. Except the case of SiS-500, in the other five cases we noticed a strong coincidence between theory and experiment, and the data is presented in Figure 11b. Furthermore, our experimental observation of grating period for the substrates SiS-10, SiS-25, SiS-50, SiS-100, and SiS-200 were in excellent
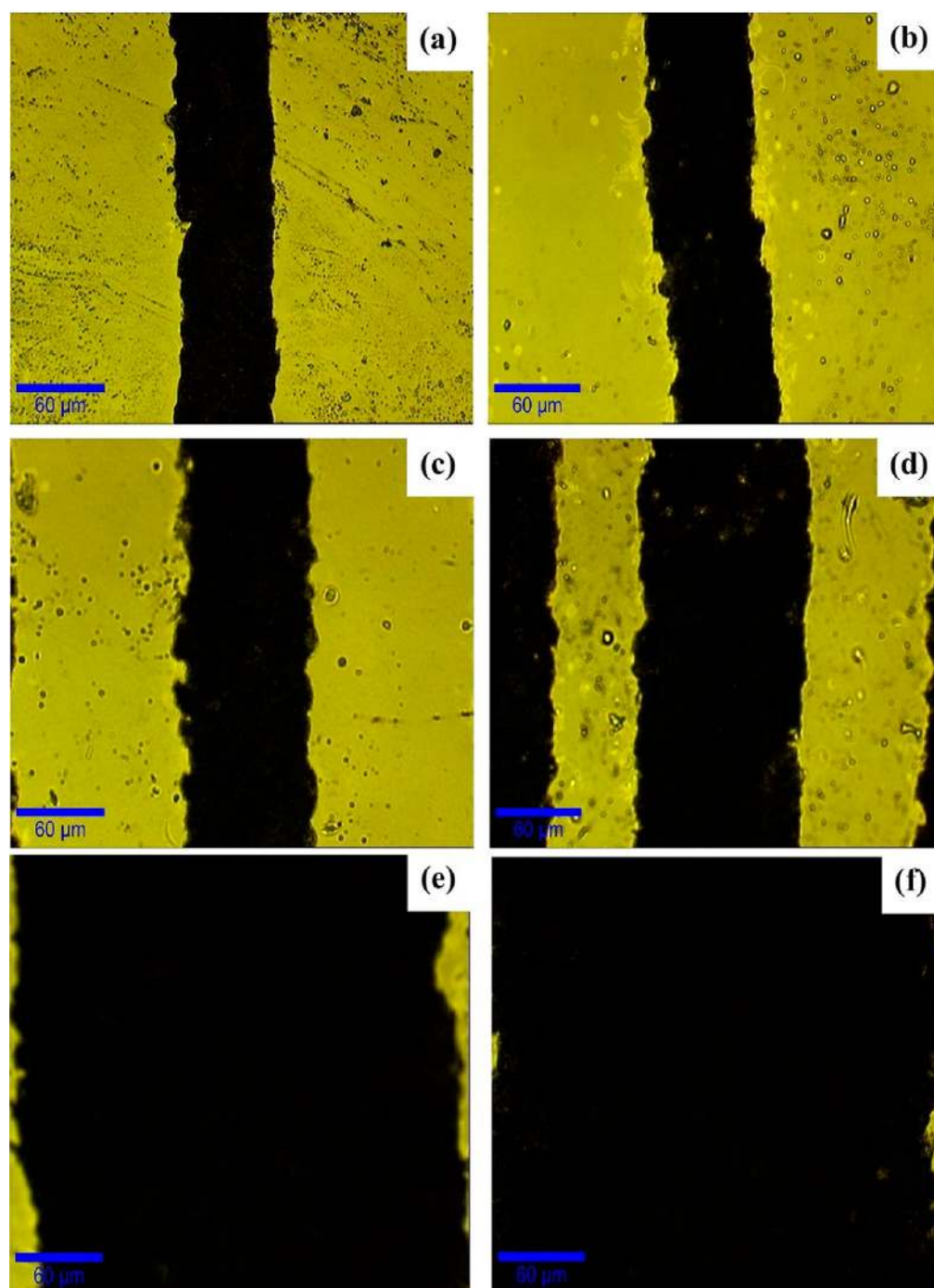
Figure 10. Microscopic images of the laser drawn single line on silicon surface with (a) 10, (b) 25, (c) 50, (d) 100, (e) 200, and (f) 500 μJ.

agreement with the prediction of the fluence dependence of grating period reported by Miyaji et al.[90] However, we observed disagreement in the case of SiS-500. The observed discrepancy for SiS-500 could be due to the large increment of beam spot on the target Si surface at that particular input pulse energy. We expect that large number of pulses per spot created a different grating period. From the experimental observations we could conclude that better yield of Si NPs with tunability of PL peak and self-organized HSFLIPSS fabricated through the ablation of silicon in acetone occur below the input laser energy 500 μJ. We could observe good agreement between the theory and experiment for periodic silicon gratings, which were fabricated below the pulse energy of 500 μJ.

Very recent reports suggest the true potential of Si NPs and NSs. Bagga et al.[91] studied protein-functionalized luminescent Si NPs prepared using infrared ultrafast laser ablation of silicon in an aqueous solution of *Staphylococcus aureus* protein A. Their detailed studies clearly revealed that the protein A-capped Si NPs are suitable for biological applications. Blandin et al.[92] prepared ultrapure Si-based colloidal nanoparticles using ultrafast ablation in liquids. They demonstrated the possibility of fast synthesis of nonaggregated, low-size-dispersed, crystalline Si-based NPs, and because of their superior purity and PL properties they argue that these NPs possess potential for biological in vivo applications such as drug vectoring and therapeutics. Simitzi et al.[93] reported the culturing of PC12

7147

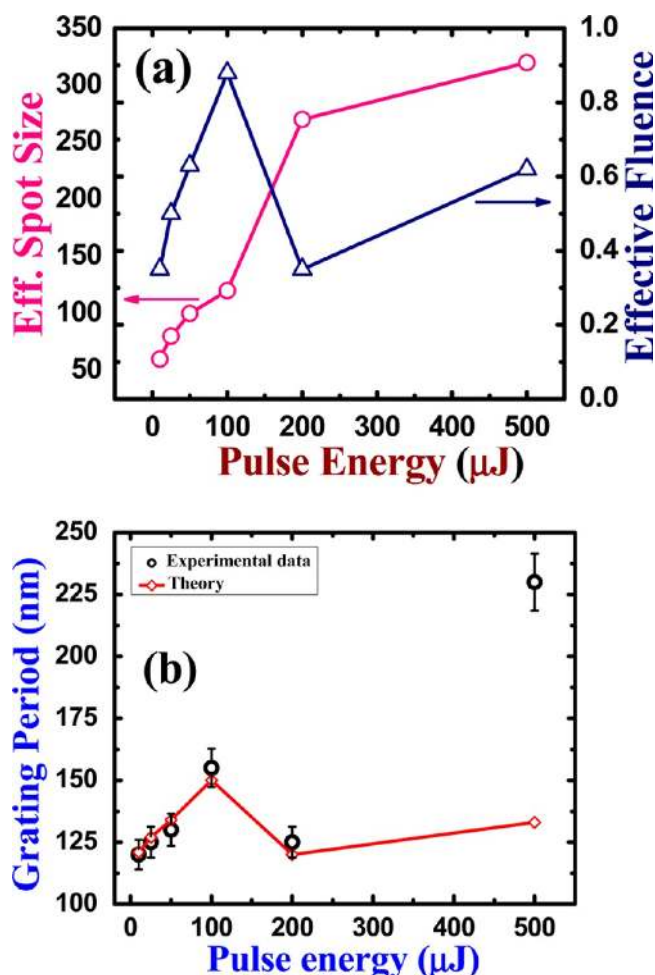dx.doi.org/10.1021/jp501152x | J. Phys. Chem. C 2014, 118, 7139−7151

Figure 11. (a) Estimated spot sizes (pink-open circles) and corresponding fluences (blue-open triangles) for each input laser energies and (b) comparison of experimental and theoretical data of HSFL grating period (Λ) as the function of pulse energy.

Table 1. Summary of Theoretically Calculated Values of Electron Density (N_e) and Complex Refractive Indices (n^*)

S. No.	pulse energy (μJ)	electron density (N_e) $\times 10^{21}$ cm^{-3}	complex refractive index (n^*)
1	10	0.94	3.31
2	25	1.34	3.14
3	50	1.72	2.98
4	100	2.38	2.67
5	200	0.92	3.32
6	500	1.69	2.99

cells on patterned Si surfaces consisting of arrays of microcones, which exhibited different geometrical characteristics and surface chemistry. It was demonstrated that microcones could influence the differentiation of PC12 cells. Wang et al.[94] reported seed-free growth of diamond patterns on Si surfaces achieved by surface patterning using direct writing with fs pulses followed by laser-assisted combustion synthesis. They believe that such patterns on nondiamond surfaces have potential applications such as cutting tools, protective coatings, heat sinks, etc. Li et al.[95] assembled Si nanoflowers from Si nanospheres created using ultrafast ablation, and they demonstrated significant, enhanced second harmonic generation. Dasog et al.[96] argue that trace N$_2$ and O$_2$ contamination in nanocrystalline Si

provided a rational explanation for the blue PL observed. Their study, they argue further, definitively demonstrated that the Si NCs prepared by solution methods contain N$_2$/O$_2$ and that exposure to N$_2$-containing reagents in the presence of O$_2$ induces blue PL.

Our future research studies will (a) incorporate further tuning the PL emission peak using different scanning procedures, using ps pulses for ablation, etc., (b) investigate the ultrafast nonlinear optical properties of these Si NPs, (c) include applications of Si NSs for SERS after coating them with thin layers either Ag or Au, and (d) study the fs/ps laser irradiation effects on the generated NP's to create uniform particles <5 nm in size for photonic applications.

■ CONCLUSIONS

In summary, the dependence of the yield of the Si NPs and the periodicity of the produced HSFLIPSS on the input laser energy in the process of double/multiple line ablation in acetone were investigated systematically through the estimation of effective spot size on the target and corresponding fluences. Size dependent tunability of the PL peak position of the Si NPs was discussed in detail. Complex refractive index and electron density in conduction band were estimated from the effective fluence, and a theoretically estimated period of gratings agreed well with the experimentally observed periodicity for the substrates SiS-10, SiS-25, SiS-50, SiS-100, and SiS-200 except for SiS-500, which was discussed. The present set of experiments revealed that, to obtain a better yield of the Si NPs along with a superior tunability of the PL peak and self-organized HSFLIPSS, ablation of silicon in acetone should be performed below the input laser energy of 500 μJ.

■ AUTHOR INFORMATION

Corresponding Author
*(S.V.R.) E-mail: soma_venu@yahoo.com or soma_venu@uohyd.ac.in. Phone: 91-40-23138811.

Notes
The authors declare no competing financial interest.
$^{\parallel}$(S.P.T.) Retired in April 2013.

■ ACKNOWLEDGMENTS

■ REFERENCES

(1) Pavesi, L.; Dal Negro, L.; Mazzoleni, C.; Franzoá, G.; Priolo, F. Optical Gain in Silicon Nanocrystals. *Nature* **2000**, *408*, 440−444.

(2) Robert, J. W.; George, I. B.; Harry, A. A. Field-Effect Electroluminescence in Silicon Nanocrystals. *Nat. Mater.* **2005**, *4*, 143−146.

(3) Prashant, V. K. Quantum Dot Solar Cells. Semiconductor Nanocrystals as Light Harvesters. *J. Phys. Chem. C* **2008**, *112*, 18737−18753.

(4) Dai, Q.; Duty, C. E.; Hu, M. Z. Semiconductor Nanocrystals Based White Light-Emitting Diodes. *Small* **2010**, *6*, 1577−1588.

(5) Mueller, A. H.; Petruska, M. A.; Achermann, M.; Werder, D. J.; Akhadov, E. A.; Koleske, D. D.; Hoffbauer, M. A.; Klimov, V. I. Multicolor Light-Emitting Diodes Based on Semiconductor Nanocrystals Encapsulated in GaN Charge Injection Layers. *Nano Lett.* **2005**, *5*, 1039−1044.

(6) Park, J. H.; Gu, L.; von Maltzahn, G.; Ruoslahti, E.; Bhatia, S. N.; Sailor, M. J. Biodegradable Luminescent Porous Silicon Nanoparticles for in vivo Applications. *Nat. Mater.* **2009**, *8*, 331−336.

(7) He, Y.; Kang, Z. H.; Li, Q. S.; Tsang, C. H. A.; Fan, C. H.; Lee, S. T. Ultrastable, Highly Fluorescent, and Water-Dispersed Silicon-Based Nanospheres as Cellular Probes. *Angew. Chem., Int. Ed.* **2009**, *48*, 128− 132.

(8) Bettotti, P.; Cazzanelli, M.; Dal Negro, L.; Danese, B.; Gaburro, Z.; Oton, C. J.; Vijaya Prakash, G.; Pavesi, L. Silicon Nanostructures for Photonics. *J. Phys.: Condens. Matter* **2002**, *14*, 8253−8281.

(9) Švrček, V.; Fujiwara, H.; Kondo, M. Top-down Silicon Nanocrystals and a Conjugated Polymer-Based Bulk Heterojunction: Optoelectronic and Photovoltaic Applications. *Acta Mater.* **2009**, *57*, 5986−5995.

(10) Kovalev, D.; Gross, E.; Künzner, N.; Koch, F.; Timoshenko, V. Y.; Fujii, M. Resonant Electronic Energy Transfer from Excitons Confined in Silicon Nanocrystals to Oxygen Molecules. *Phys. Rev. Lett.* **2002**, *89*, 137401.

(11) Chirvony, V.; Chyrvonaya, A.; Ovejero, J.; Matveeva, E.; Goller, B.; Kovalev, D.; Huygens, A.; de Witte, P. Surfactant-Modified Hydrophilic Nanostructured Porous Silicon for The Photosensitized Formation of Singlet Oxygen in Water. *Adv. Mater.* **2007**, *19*, 2967− 2972.

(12) Zurauskiene, N.; Asmontas, S. S.; Dargys, A.; Kundrotas, J.; Janssen, G.; Goovaerts, E.; Marcinkevicius, S.; Koenraad, P. M.; Wolter, J. H.; Leon, R. P. Semiconductor Nanostructures for Infrared Applications. *Solid State Phenom.* **2003**, *99*, 99−108.

(13) Lutskii, V. N. Quantum Size Effect: Present State and Perspectives of Experimental Investigations. *Phys. Status Solidi A* **1970**, *1*, 199−220.

(14) Manasreh, O. *Semiconductor Heterojunctions and Nanostructures*; McGraw Hill: New York, 2005.

(15) Delley, B.; Steigmeier, E. F. Quantum Confinement in Si Nanocrystals. *Phys. Rev. B.* **1993**, *47*, 1397−1400.

(16) Öğüt, S.; Chelikowsky, J. R. Quantum Confinement and Optical Gaps in Si Nanocrystals. *Phys. Rev. Lett.* **1997**, *79*, 1770−1773.

(17) Ledoux, G.; Gong, J.; Huisken, F.; Guillois, O.; Reynaud, C. Photoluminescence of Size-Separated Silicon Nanocrystals: Confirmation of Quantum Confinement. *Appl. Phys. Lett.* **2002**, *80*, 4834−4836.

(18) Chen, X. Y.; Lu, Y. F.; Wu, Y. H.; Cho, B. J.; Liu, M. H.; Dai, D. Y.; Song, W. D. Mechanisms of Photoluminescence from Silicon Nanocrystals Formed by Pulsed-Laser Deposition in Argon and Oxygen Ambient. *J. Appl. Phys.* **2003**, *93*, 6311−6319.

(19) Burda, C.; Chen, X.; Narayanan, R.; El-Sayed, M. A. Chemistry and Properties of Nanocrystals of Different Shapes. *Chem. Rev.* **2005**, *105*, 1025−1102.

(20) Vijaya Prakash, G.; Cazzanelli, M.; Gaburro, Z.; Pavesi, L.; Iacona, F.; Franzó, G.; Priolo, F. Nonlinear Optical Properties of Silicon Nanocrystals Grown by Plasma-Enhanced Chemical Vapor Deposition. *J. Appl. Phys.* **2002**, *91*, 4607.

(21) Vijayalakshmi, S.; Grebel, H.; Iqbal, Z.; White, C. W. Artificial Dielectrics: Nonlinear Properties of Si Nanoclusters formed by Ion-Implantation in SiO_2 Glassy Matrix. *J. Appl. Phys.* **1998**, *84*, 6502− 6506.

(22) Figliozzi, P.; Sun, L.; Jiang, Y.; Matlis, N.; Mattern, B.; Downer, M. C.; With-row, S. P.; White, C. W.; Mochán, W. L.; Mendoza, B. S. Single-Beam and Enhanced Two-Beam Second-Harmonic Generation from Silicon Nanocrystals by Use of Spatially Inhomogeneous Femtosecond Pulses. *Phys. Rev. Lett.* **2005**, *94*, 47401.

(23) Rahman, I. A.; Padavettan, V. Synthesis of Silica Nanoparticles by Sol-Gel: Size-Dependent Properties, Surface Modification, and Applications in Silica-Polymer Nanocomposites: A Review. *J. Nanomat.* **2012**, *2012*, 132424.

(24) Kenyon, A. J.; Trwoga, P. F.; Pitt, C. W. The Origin of Photoluminescence from Thin Films of Silicon-Rich Silica. *J. Appl. Phys.* **1996**, *79*, 9291−9300.

(25) Chen, X. Y.; Lu, Y. F.; Tang, L. J.; Wu, Y. H.; Cho, B. J.; Xu, X. J.; Dong, J. R.; Song, W. D. Annealing and Oxidation of Silicon Oxide Films Prepared by Plasma Enhanced Chemical Vapor Deposition. *J. Appl. Phys.* **2005**, *97*, 014913.

(26) Benyoucef, M.; Kubell, M.; Sun, J. M.; Zhong, G. Z.; Fan, X. W. Raman Scattering and Photoluminescence Studies on Si/SiO_2 Superlattices. *J. Appl. Phys.* **2001**, *89*, 7903−7907.

(27) Chaudhari, P. S.; Bhave, T. M.; Kanjilal, D.; Bhoraskar, S. V. Swift Heavy Ion Induced Growth of Nanocrystalline Silicon in Silicon Oxide. *J. Appl. Phys.* **2003**, *93*, 3486−3489.

(28) Liong, W. L.; Sreekantan, S.; Hutagalung, S. D. Effect of Concentration of Sodium Borohydate on the Synthesis of Silicon Nanoparticles via Microemulsion Route. *World Acad. Sci., Eng. Technol.* **2009**, *59*, 419−422.

(29) Umezu, I.; Minami, H.; Senoo, H.; Sugimura, A. Synthesis of PhotoluminescentColloidal Silicon Nanoparticles By Pulsed Laser Ablation in Liquids. *J. Phys. Conf. Ser.* **2007**, *59*, 392−395.

(30) Huang, C. C.; Chuang, K. Y.; Huang, C. J.; Liu, T. M.; Yeh, C. S. Graphite-Shelled Si Nanoparticles and Their Au/Si Heterodimers: Preparation, Photoluminescence, and Second Harmonic Generation. *J. Phys. Chem. C* **2011**, *115*, 9952−9960.

(31) Švrcek, V.; Sasaki, T.; Shimizu, Y.; Koshizaki, N. Blue Luminescent Silicon Nanocrystals Prepared by ns Pulsed Laser Ablation in Water. *Appl. Phys. Lett.* **2006**, *89*, 213113.

(32) Du, X. W.; Qin, W. J.; Lu, Y. W.; Han, X.; Fu, Y. S.; Hu, S. L. Face-Centered-Cubic Si Nanocrystals Prepared By Microsecond Pulsed Laser Ablation. *J. Appl. Phys.* **2007**, *102*, 013518.

(33) Shirahata, N.; Linford, M. R.; Furumi, S.; Pei, L.; Sakka, Y.; Gatesb, R. J.; Asplund, M. C. Laser-Derived One-Pot Synthesis of Silicon Nanocrystals Terminated with Organic Monolayers. *Chem. Commun.* **2009**, *31*, 4684−4686.

(34) Švrcek, V.; Sasaki, T.; Katoh, R.; Koshizaki, N. Aging Effect on Blue Luminescent Silicon Nanocrystals Prepared By Pulsed Laser Ablation of Silicon Wafer in De-ionized Water. *Appl. Phys. B: Laser Opt.* **2009**, *94*, 133−139.

(35) Semaltianos, N. G.; Logothetidis, S.; Perrie, W.; Romani, S.; Potter, R. J.; Edwardson, S. P.; French, P.; Sharp, M.; Dearden, G.; Watkins, K. G. Silicon Nanoparticles Generated by Femtosecond Laser Ablation in a Liquid Environment. *J. Nanopart. Res.* **2010**, *12*, 573− 580.

(36) Popovic, D. M.; Chai, J. S.; Zekic, A. A.; Trtica, M.; Momcilovic, M.; Maletic, S. Synthesis of Silicon-Based Nanoparticles by 10.6 μm Nanosecond CO_2 Laser Ablation in Liquid. *Laser Phys. Lett.* **2013**, *10*, 026001.

(37) Yang, S. K.; Cai, W.; Zhang, H.; Xu, X.; Zeng, H. Size and Structure Control of Si Nanoparticles by Laser Ablation in Different Liquid Media and Further Centrifugation Classification. *J. Phys. Chem. C* **2009**, *113*, 19091−19095.

(38) Yang, S. K.; Cai, W.; Liu, G.; Zeng, H.; Liu, P. Optical Study of Redox Behavior of Silicon Nanoparticles Induced by Laser Ablation in Liquid. *J. Phys. Chem. C* **2009**, *113*, 6480−6484.

(39) Chen, F.; Zhang, D.; Yang, Q.; Yong, J.; Du, G.; Jinhai, S.; Yun, F.; Hou, X. Bioinspired Wetting Surface via Laser Microfabrication. *ACS Appl. Mater. Interfaces* **2013**, *5*, 6777−6792.

(40) Blandin, P.; Ksenia, A. M.; Maxim, B. G.; Sanchez-Royo, J. F.; Vladimir, S. C.; Marc, S.; Victor, Y. T.; Andrei, V. K. Femtosecond Laser Fragmentation from Water-Dispersed Microcolloids: Toward Fast Controllable Growth of Ultrapure Si-Based Nanomaterials for Biological Applications. *J. Mater. Chem. B* **2013**, *1*, 2489−2495.

(41) Dezhi, T.; Zhijun, M.; Xu, B.; Ye, D.; Guohong, M.; Min, H.; Zuanming, J.; Qiu, J. Surface Passivated Silicon Nanocrystals with Stable Luminescence Synthesized by Femtosecond Laser Ablation in Solution. *Phys. Chem. Chem. Phys.* **2011**, *13*, 20255−20261.

(42) Intartaglia, R.; Das, G.; Bagga, K.; Gopala Krishnan, A.; Genovese, A.; Povia, M.; Di Fabrizio, E.; Cingolani, R.; Diaspro, A.; Brandi, F. Laser Synthesis of Ligand-Free Bimetallic Nanoparticles for Plasmonic Applications. *Phys. Chem. Chem. Phys.* **2013**, *15*, 3075− 3082.

(43) Sallé, B.; Gobert, O.; Meynadier, P.; Perdrix, M.; Petite, G.; Semerok, A. Femtosecond and Picosecond Laser Microablation:

Ablation Efficiency and Laser Microplasma Expansion. *Appl. Phys. A: Mater. Sci. Process.* **1999**, *69*, S381−S383.

(44) Afanasiev, Y. V.; Chichkov, B. N.; Isakov, V. A.; Kanavin, A. P.; Uryupin, S. A. Thermal Regime of Laser Ablation of Metals by Ultrashort Pulses of Low Fluence. *J. Russ. Laser Res.* **1999**, *20*, 189−201.

(45) Von der Linde, D.; Sokolowski-Tinten, K.; Bialkowski, J. Laser−Solid Interaction in The Femtosecond Time Regime. *Appl. Surf. Sci.* **1997**, *109/110*, 1−10.

(46) Intartaglia, R.; Bagga, K.; Scotto, M.; Diaspro, A.; Brandi, F. Luminescent Silicon Nanoparticles Prepared by Ultrashort Pulsed Laser Ablation in Liquid for Imaging Applications. *Opt. Mater. Express* **2012**, *2*, 510−518.

(47) Intartaglia, R.; Bagga, K.; Brandi, F.; Das, G.; Genovese, A.; Di Fabrizio, E.; Diaspro, A. Optical Properties of Femtosecond Laser-Synthesized Silicon Nanoparticles in Deionized Water. *J. Phys. Chem. C* **2011**, *115*, 5102−5107.

(48) Krishna, P. G.; Hamad, S.; Tewari, S. P.; Sreedhar, S.; Prasad, M. D.; Rao, S. V. Silver Nano-Entities Through Ultrafast Double Ablation in Aqueous Media for Surface Enhanced Raman Scattering and Photonics Applications. *J. Appl. Phys.* **2013**, *113*, 073106.

(49) Fauchet, P. M.; Siegman, A. E. Surface Ripples on Silicon and Gallium Arsenide under Picosecond Laser Illumination. *Appl. Phys. Lett.* **1982**, *40*, 824−826.

(50) Sipe, J. E.; Young, J. F.; Preston, J. S.; Vandriel, H. M. Laser-Induced Periodic Surface Structure. I. Theory. *Phys. Rev. B* **1983**, *27*, 1141−1154.

(51) Huang, M.; Zhao, F.; Cheng, Y.; Xu, N.; Xu, Z. Origin of Laser-Induced Near Subwavelength Ripples: Interference Between Surface Plasmons and Incident Laser. *ACS Nano* **2009**, *3*, 4062−4070.

(52) Varlamova, O.; Costache, F.; Reif, J.; Bestehorn, M. Self-Organized Pattern Formation upon Femtosecond Laser Ablation by Circularly Polarized Light. *Appl. Surf. Sci.* **2006**, *252*, 4702−4706.

(53) Borowiec, A.; Haugen, H. K. Subwavelength Ripple Formation on the Surfaces of Compound Semiconductors Irradiated with Femtosecond Laser Pulses. *Appl. Phys. Lett.* **2003**, *82*, 4462−4464.

(54) Krishna, P. G.; Hamad, S.; Sreedhar, S.; Tewari, S. P.; Rao, S. V. Fabrication and Characterization of Aluminum Nanostructures and Nanoparticles Obtained Using Femtosecond Ablation Technique. *Chem. Phys. Lett.* **2012**, *530*, 93−97.

(55) Hamad, S.; Krishna, P. G.; Sreedhar, S.; Tewari, S. P.; Rao, S. V. Femtosecond and Picosecond Ablation of Aluminum for Synthesis of Nanoparticles and Nanostructures and Their Optical Characterization. *Proc. SPIE* **2012**, *8245*, 82450L.

(56) Rao, S. V.; Podagatlapalli, G. K.; Hamad, S. Ultrafast Laser Ablation in Liquids for Nanomaterials and Applications. *J. Nanosci. Nanotechnol.* **2014**, *14*, 1364−1388.

(57) Hamad, S.; Krishna, P. G.; Tewari, S. P.; Rao, S. V. Influence of Picosecond Multiple/Single Line Ablation on Copper Nanoparticles Fabricated for Surface Enhanced Raman Spectroscopy and Photonics Applications. *J. Phys. D: Appl. Phys.* **2013**, *46*, 485501.

(58) Menendez-Manjon, A.; Wagener, P.; Barcikowski, S. Transfer-Matrix Method for Efficient Ablation by Pulsed Laser Ablation and Nanoparticle Generation in Liquids. *J. Phys. Chem. C* **2011**, *115*, 5108−5114.

(59) David, J. H.; Costas, P. G.; Tae, Y. C. Efficiency of Silicon Micromachining By Femtosecond Laser Pulses in Ambient Air. *J. Appl. Phys.* **2006**, *99*, 083101.

(60) Faraci, G.; Gibilisco, S.; Russo, P.; Pennisi, A. R.; Rosa, S. L. Modified Raman Confinement Model for Si Nanocrystals. *Phys. Rev. B* **2006**, *73*, 033307.

(61) Islam, M. N.; Pradhan, A.; Kumar, S. Effects of Crystallite Size Distribution on The Raman Scattering Profiles of Silicon Nanostructures. *J. Appl. Phys.* **2005**, *98*, 024309.

(62) Zhaoa, Z. X.; Cui, R. Q.; Meng, F. Y.; Zhao, B. C.; Yu, H. C.; Zhou, Z. B. Nanocrystalline Silicon Thin Films Prepared by RF Sputtering at Low Temperature and Heterojunction Solar Cell. *Mater. Lett.* **2004**, *58*, 3963−3966.

(63) Saxena, N.; Kumar, P.; Avinash, A.; Dinakar, K. Lattice Distortion in Ion Beam Synthesized Silicon Nanocrystals in SiOx Thin Films. *Phys. Status Solidi A* **2012**, *209*, 283−288.

(64) Zhang, W.; Zhang, S.; Liu, Y.; Chen, T. Evolution of Si Suboxides into Si Nanocrystals During Rapid Thermal Annealing as Revealed By XPS and Raman Studies. *J. Cryst. Growth* **2009**, *311*, 1296−1301.

(65) Glover, T. E. Hydrodynamics of Particle Formation Following Femtosecond Laser Ablation. *J. Opt. Soc. Am. B* **2003**, *20*, 125−131.

(66) Kanemitsu, Y.; Nakada, I.; Kuroda, H. Picosecond Laser-Induced Anomalous Crystallization in Amorphous-Silicon. *Appl. Phys. Lett.* **1985**, *47*, 939.

(67) Rosso-Vasic, M.; Spruijt, E.; Popovic, Z.; Overgaag, K.; VanLagen, B.; Grandidier, B.; Vanmaekelbergh, D.; Dominguez-Gutierrez, D.; De Cola, L.; Zuilhof, H. Amine-Terminated Silicon Nanoparticles: Synthesis, Optical Properties and Their Use in Bioimaging. *J. Mater. Chem.* **2009**, *19*, 5926−5933.

(68) Intartaglia, R.; Bagga, K.; Genovese, A.; Athanassia, A.; Roberto, C.; Diaspro, A.; Brandi, F. Influence of Organic Solvent on Optical and Structural Properties of Ultra-Small Silicon Dots Synthesized by UV Laser Ablation in Liquid. *Phys. Chem. Chem. Phys.* **2012**, *14*, 15406−15411.

(69) Kovalev, D.; Heckler, H.; Polisski, G.; Koch, F. Optical Properties of Si Nanocrystals. *Phys. Status Solidi* **1999**, *215*, 871−932.

(70) Svrcek, V.; Mariotti, D.; Kondo, M. Ambient-Stable Blue Luminescent Silicon Nanocrystals Prepared by Nanosecond-Pulsed Laser Ablation in Water. *Opt. Express* **2009**, *17*, 520−527.

(71) Mita, D.; Yang, Z.; Sarah, R.; Tonya, M. A.; Faramus, A.; Mani, P. S.; Elayaraja, M.; Susan, M. K.; Richard, D. T.; Jonathan, G. C. V. Chemical Insight into the Origin of Redand Blue Photoluminescence Arising from Freestanding Silicon Nanocrystals. *ACS Nano* **2013**, *7*, 2676−2685.

(72) Sabri, A.; Okyay, A. K.; Bulend, O. Post-Treatment of Silicon Nanocrystals Produced by Ultra-Short Pulsed Laser Ablation in Liquid: Toward Blue Luminescent Nanocrystal Generation. *J. Phys. Chem. C* **2012**, *116*, 3432−3436.

(73) Mansour, N.; Momeni, A.; Karimzadeh, R.; Amini, M. Surface Effects on the Luminescence Properties of Colloidal Silicon Nano-crystals in Water. *Phys. Scr.* **2013**, *87*, 035701.

(74) Preston, J. S.; van Driel, H. M.; Sipe, J. E. Pattern Formation during Laser Melting of Silicon. *Phys. Rev. B* **1989**, *40*, 3942−3957.

(75) Wagner, R.; Gottmann, J.; Horn, A.; Kreutz, E. W. Subwavelength Ripple Formation Induced by Tightly Focused Femtosecond Laser Radiation. *Appl. Surf. Sci.* **2006**, *252*, 8576−8579.

(76) Le Harzic, R.; Schuck, H.; Sauer, D.; Anhut, T.; Riemann, I.; König, K. Sub-100 nm Nanostructuring of Silicon by Ultrashort Laser Pulses. *Opt. Express* **2005**, *13*, 6651−6656.

(77) Miyaji, G.; Miyazaki, K. Role of Multiple Shots of Femtosecond Laser Pulses in Periodic Surface Nano Ablation. *Appl. Phys. Lett.* **2013**, *103*, 071910.

(78) Sokolowski-Tinten, K.; Bialkowski, J.; Cavalleri, A.; von der Linde, D.; Oparin, A.; Meyer-ter-Vehn, J.; Anisimov, S. I. Transient States of Matter During Short Pulse Laser Ablation. *Phys. Rev. Lett.* **1998**, *81*, 224−227.

(79) Gemini, L.; Hashida, M.; Shimizu, M.; Miyasaka, Y.; Inoue, S.; Tokita, S.; Limpouch, J.; Mocek, T.; Sakabe, S. Metal-Like Self-Organization of Periodic Nanostructures on Silicon and Silicon Carbide under Femtosecond Laser Pulses. *J. Appl. Phys.* **2013**, *114*, 194903.

(80) Miyazaki, K.; Miyaji, G. Mechanism and Control of Periodic Surface Nanostructure Formation with Femtosecond Laser Pulses. *Appl. Phys. A: Mater. Sci. Process.* **2014**, *114*, 177−185.

(81) Derrien, T. J. Y.; Itina, T. E.; Torres, R.; Sarnet, T.; Sentis, M. Possible Surface Plasmon Polariton Excitation under Femtosecond Laser Irradiation of Silicon. *J. Appl. Phys.* **2013**, *114*, 083104.

(82) Liu, P.; Jiang, L.; Hu, J.; Han, W.; Lu, Y. Direct Writing Anisotropy on Crystalline Silicon Surface by Linearly Polarized Femtosecond Laser. *Opt. Lett.* **2013**, *38*, 1969−1971.

(83) Le Harzic, R.; Dörr, D.; Sauer, D.; Stracke, F.; Zimmermann, H. Generation of High Spatial Frequency Ripples on Silicon under Ultrashort Laser Pulses Irradiation. *Appl. Phys. Lett.* **2011**, *98*, 211905.

(84) Ganeev, R. A.; Lei, D. Y.; Hutchison, C.; Witting, T.; Frank, F.; Okell, W. A.; Roschuk, T. R.; Maier, S. A.; Tisch, J. W. G.; Marangos, J. P. Extended Homogeneous Nanoripple Formation during Interaction of High-Intensity Few-Cycle Pulses with a Moving Silicon Wafer. *Appl. Phys. A: Mater. Sci. Process.* **2013**, *112*, 457−462.

(85) Sokolowski-Tinten, K.; von der Linde, D. Generation of Dense Electron-Hole Plasmas in Silicon. *Phys. Rev. B* **2000**, *61*, 2643−2650.

(86) Le Harzic, R.; Dörr, D.; Sauer, D.; Stracke, F.; Zimmermann, H. Generation of High Spatial Frequency Ripples on Silicon under Ultrashort Laser Pulses Irradiation. *Appl. Phys. Lett.* **2011**, *98*, 211905.

(87) E. D. Palik., Ed. *Handbook of Optical Constants of Solids*; Academic: Orlando, FL, 1985.

(88) Sabbah, A. J.; Riffe, D. M. Femtosecond Pump-Probe Reflectivity Study of Silicon Carrier Dynamics. *Phys. Rev. B* **2002**, *66*, 165217.

(89) Barcikowski, S.; Menéndez-Manjón, A.; Chichkov, B.; Brikas, M.; Gediminas, R. Generation of Nanoparticle Colloids by Picosecond and Femtosecond Laser Ablations in Liquid Flow. *Appl. Phys. Lett.* **2007**, *91*, 083113.

(90) Miyaji, G.; Miyazaki, K.; Zhang, K.; Yoshifuji, T.; Fujita, J. Mechanism of Femtosecond-Laser-Induced Periodic Nanostructure Formation on Crystalline Silicon Surface Immersed in Water. *Opt. Express* **2012**, *20*, 14848−14856.

(91) Bagga, K.; Barchanski, A.; Intartaglia, R.; Dante, S.; Marotta, R.; Diaspro, A.; Sajti, C. L.; Brandi, F. Laser-Assisted Synthesis of Staphylococcus Aureus Protein-Capped Silicon Quantum Dots as Bio-Functional Nanoprobes. *Laser Phys. Lett.* **2013**, *10*, 065603.

(92) Blandin, P.; Maximova, K. A.; Gongalsky, M. B.; Sanchez-Royo, J. F.; Chirvony, V. S.; Sentis, M.; Timoshenko, V. U.; Kabashin, A. V. Femtosecond Laser Fragmentation from Water-Dispersed Micro-colloids: Toward Fast Controllable Growth of Ultrapure Si-Based Nanomaterials for Biological Applications. *J. Mater. Chem. B* **2013**, *1*, 2489−2495.

(93) Simitzi, C.; Stratakis, E.; Fotakis, C.; Athanassakis, I.; Ranella, A. Microconical Silicon Structures Influence NGF induced PC12 Cell Morphology. *Tissue Eng. Regener. Med.* **2013**, DOI: 10.1002/term.1853.

(94) Wang, M.; Zhou, Y. S.; Xie, Z. Q.; Gao, Y.; He, X. N.; Jiang, L.; Lu, Y. F. Seed-Free Growth of Diamond Patterns on Silicon Predefined by Femtosecond Laser Direct Writing. *Cryst. Growth Des.* **2013**, *13*, 716−722.

(95) Li, C. Q.; Zhang, C. Y.; Huang, Z. S.; Li, X. F.; Dai, Q. F.; Lan, S.; Tie, S. L. Assembling of Silicon Nanoflowers with Significantly Enhanced Second Harmonic Generation Using Silicon Nanospheres Fabricated by Femtosecond Laser Ablation. *J. Phys. Chem. C* **2013**, *117*, 24625−24631.

(96) Dasog, M.; Yang, Z.; Regli, S.; Atkins, T. M.; Faramus, A.; Singh, M. P.; Muthuswamy, E.; Kauzlarich, S. M.; Tilley, R. D.; Veinot, J. G. C. Chemical Insight into the Origin of Red and Blue Photo-luminescence Arising from Freestanding Silicon Nanocrystals. *ACS Nano* **2013**, *7*, 2676−2685.